

Direct-Conversion RF Receiver Design

Won Namgoong, *Member, IEEE*, and Teresa H. Meng, *Fellow, IEEE*

Abstract—Direct-conversion radio-frequency receiver architecture promises superior performances in power, size, and cost over existing superheterodyne-based receivers. The use of direct-conversion receiver (DCR) architecture, however, has been limited due to two well-known problems, namely, the $1/f$ noise and the direct-current offset noise, to which conventional architectures are less sensitive. This paper analyzes these noise effects on reception performance of a DCR with alternating-current (ac) coupling filter in the receive path. A mathematical treatment of the performance of a DCR is provided. A performance bound of a DCR given its $1/f$ noise roll-off frequency and ac-coupling filter cut-off frequency is first obtained using vector coding. Then, the performance of a more practical adaptive reception method using a linear equalizer is discussed. Adaptability is especially important in rapidly time-varying channels such as in the wireless environment. Linear equalizer is effective at signal-to-noise ratios (SNRs) below 9 dB, but its performance degrades significantly at larger SNR. To achieve high performance at large SNR (>9 dB), a spectrum shaping method using line codes for direct-conversion reception is proposed. This method achieves near-optimum direct-conversion reception at high SNR while maintaining low complexity and adaptability at the receiver.

Index Terms—Analog systems, communication systems, equalizers, receivers.

I. INTRODUCTION

NEARLY all existing radio receivers are designed based on a superheterodyne architecture [1]. In its simplest form, this receiver architecture filters the received radio frequency (RF) signal and converts it to a lower intermediate frequency (IF) by mixing with an offset local-oscillator (LO_1) as shown in Fig. 1. The resulting IF signal is then amplified before shifting to the baseband, where it is quantized and demodulated. Signal amplification at an intermediate frequency, however, requires IF filters to be biased with large currents, causing substantial power dissipation. Further, these filters need many off-chip passive components, adding to receiver size and cost. Another important drawback of a superheterodyne architecture is that an unwanted signal, situated at an intermediate frequency above the LO_1 frequency, is also translated to the IF. Removal of this undesired signal, known as the image signal, requires a highly selective and expensive analog RF filter. The stringent RF filter requirements can be relaxed by using a dual-conversion (two IFs) or a triple-conversion (three IFs) receiver at the cost of added receiver complexity and size.

Paper approved by R. A. Valenzuela, the Editor for Transmission Systems of the IEEE Communications Society. Manuscript received February 20, 1998; revised May 30, 1999.

W. Namgoong is with the University of Southern California, Los Angeles, CA 90089-2562 USA (e-mail: namgoong@usc.edu).

T. H. Meng is with Stanford University, Stanford, CA 94305-4070 USA (e-mail: meng@mohave.stanford.edu).

Publisher Item Identifier S 0090-6778(01)02180-8.

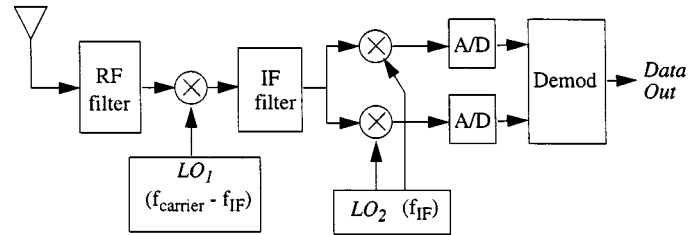


Fig. 1. Superheterodyne receiver.

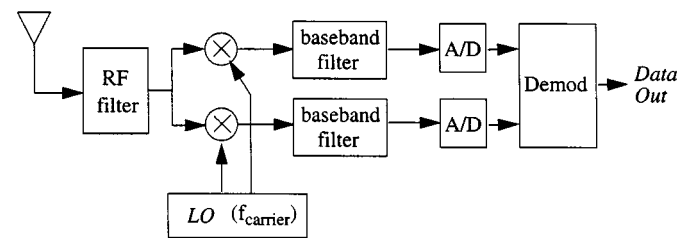


Fig. 2. DCR.

If the IF is designed to be centered at frequency zero, there is no image signal to be rejected and the analog filtering problem can be easily handled. This process of frequency translation to zero IF is called direct-conversion and is illustrated in Fig. 2. With zero IF, the desired signal is translated directly to the baseband, allowing analog-to-digital (A/D) converter and digital signal processing (DSP) circuits to perform demodulation and other ancillary functions. The direct-conversion receiver (DCR) architecture, therefore, relaxes the selectivity requirements of RF filters and eliminates all IF analog components, allowing a highly integrated, low-cost and low-power realization [1].

Despite these attractive attributes, superheterodyne-based receiver architectures are almost exclusively employed for RF signal reception. DCRs are rarely used because they can be extremely noisy, resulting in severe performance degradation compared to conventional architectures. This paper addresses the two most challenging of these noise sources, namely, the $1/f$ noise and the dc-offset noise, and analyzes their effects on reception performance. Since a mathematical treatment of the performance of a DCR has never been previously published, we first provide the performance bound of an optimal DCR, followed by the performance evaluation of an adaptive reception method using a linear equalizer. A spectral shaping method that achieves near-optimum direct-conversion performance while retaining the adaptability of a linear equalizer is then proposed. Although this spectral shaping method is not limited to a specific application, a strong motivation for its use is in wireless communications, where adaptability to rapidly changing channel conditions and low power consumption are critical issues.

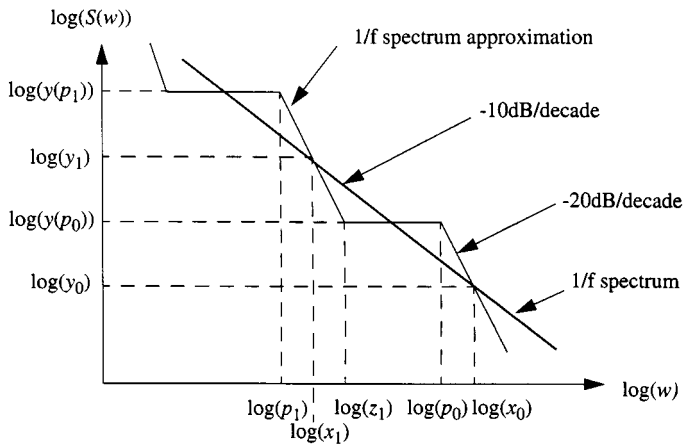


Fig. 3. Linear system model of the 1/f noise.

In Section II, the noise sources unique to DCR architectures are examined, and methods of overcoming these noise degradation and their shortcomings are discussed. In Section III, the system model for performance analysis is outlined. In Section IV, DCR architectures using various transmission and reception methods are analyzed. An example of a DCR design is also provided. Finally, conclusions are drawn in Section V.

II. NOISE SOURCES IN DIRECT-CONVERSION RF RECEIVERS

DCRs suffer from several noise sources that do not exist or are not serious in superheterodyne receivers: I/Q mismatch, even-order distortion, dc-offset, and 1/f noise. The effects of the I/Q mismatch and even-order noise distortions can generally be made sufficiently negligible with good circuit techniques. In applications with strong blocking signals, however, even-order distortion may also be significant. We do not address such applications and assume that the even-order distortion has been sufficiently attenuated. Compared to the I/Q mismatch and even-order noise distortions, the dc-offset and 1/f noise problems in a DCR are generally considered much more serious and challenging to the designers [14]. Consequently, this paper analyzes the performance degradation of a DCR resulting from the dc-offset and 1/f noise distortions only.

A. 1/f Noise

The 1/f noise (also known as flicker noise or pink noise) is an intrinsic noise phenomenon found in semiconductor devices. As the term “1/f” suggests, the noise is characterized by a spectral density that is inversely proportional to frequency. We use a linear model to approximate the 1/f noise spectrum by appropriately selecting its poles and zeros as shown in Fig. 3. Given the 1/f roll-off frequency x_0 (in radians), which is the frequency at which the 1/f noise enters the noise floor, and the maximum allowed difference in decibels between the approximating linear model spectrum and 1/f noise spectrum, the poles and zeros of the approximating linear time-invariant filter can

be recursively computed using elementary geometry. The formulas for computing these poles and zeros are provided in the appendix. The approximating linear filter is given by

$$H(j\omega) = \frac{(j\omega + z_1) \times (j\omega + z_2) \times \dots \times (j\omega + z_m)}{(j\omega + p_0) \times (j\omega + p_1) \times \dots \times (j\omega + p_m)} \times k \quad (1)$$

where z_i represents the i th zero and p_i the j th pole. A total of m zeros and $m + 1$ poles are used to model the 1/f noise and k is a scale factor to ensure that the 1/f noise enters the noise floor at the roll-off frequency x_0 . Since the 1/f noise spectral density increases without limit with decreasing frequency, an infinite number of poles and zeros would be required to model the 1/f noise. As described in Section III, however, a few decades of approximation to the 1/f power spectral density (PSD) is sufficient in our system model due to the ac-coupling filter employed in the receiver.

The coupling of the 1/f noise with the received signal occurs primarily after down-conversion to the baseband. Since the power of the baseband signal can be in the range of hundreds of microvolts root-mean-square, the 1/f noise comprises a substantial fraction of the signal power, resulting in large signal distortion. The exact 1/f roll-off frequency depends on the noise floor and the processing technology employed. The 1/f noise in metal-oxide-semiconductor technology, for example, enters the thermal noise floor at several megahertz. Since the noise floor of a DCR after down-conversion to the baseband is raised by the power gain and the noise figure of the RF and down-conversion stages, the frequency at which the 1/f noise enters the noise floor is correspondingly reduced. For example, if the RF and down-conversion stages provide a power gain of 25 dB and a noise figure of 5 dB, the noise floor is raised by 30 dB relative to the thermal noise floor and the 1/f roll-off frequency is reduced by 30 dB to several kilohertz. We refer to the 1/f noise roll-off frequency as the frequency at which the 1/f noise enters the noise floor after down-conversion to the baseband. In this paper, the performance of a DCR with 1/f roll-off frequencies of 5.0%, 10.0%, and 15.0% of the symbol frequency are considered.

In a superheterodyne-based architecture, the 1/f noise is negligible because the signal is substantially amplified at the IF. When this amplified IF signal is translated to the baseband, the power of the 1/f noise becomes insignificant relative to that of the signal.

B. DC-Offset Noise

In a DCR, an offset voltage may appear in the signal spectrum at dc. This offset voltage value dominates the signal strength by as much as 50–100 times in amplitude and, if not removed, may substantially degrade the bit-error probability. Furthermore, this offset voltage must be removed in the analog domain prior to sampling, because it otherwise saturates the baseband amplifiers, resulting in potentially devastating nonlinear signal distortion. Even if ideal baseband amplifiers are employed, an impractically large dynamic range for the A/D converter will be required to resolve the signal from the dc-offset.

The dc-offset noise arises when the LO signal leaks to the RF signal path then self-downconverts to dc. Since the LO signal is at the same frequency as the RF signal, the LO signal also leaks from the antenna during receive mode and reflects off an external object and self-downconverts to dc. This self-rectification introduces tremendous dc-offset noise after direct-conversion as the LO signal is generally many orders of magnitude stronger than the RF signal. Furthermore, the amount of dc-offset generated by the LO radiation is difficult to predict since its magnitude changes with receiver location, orientation, and time. A similar effect occurs if a strong interferer leaks into the LO port of the mixer and downconverts itself.

C. Reduction of Low-Frequency Noise

Despite the benefits of a DCR, the $1/f$ noise and dc-offset noise described above have limited its widespread use. There are basically two existing methods of overcoming some of the noise issues with direct-conversion. One approach adopted by Alcatel in their GSM receiver for removing the dc-offset noise is to average the digitized baseband signal over a window and to subtract an estimate of the dc-offset from the signal using a digital-to-analog (D/A) converter [10]. This decision-directed dc-offset removal approach requires not only a larger dynamic range for the A/D converter, which is expensive in both power and cost, but also an additional D/A converter and various extraneous analog components. The complexity of this approach compromises the benefits of low complexity and low power of a DCR.

Another approach is to use an ac-coupling filter, which has been successfully employed to reduce both the size and cost of modern pagers [2]. Employing ac-coupling is especially suitable for the paging system because the paging signal uses simple two-tone signaling (wide-band frequency-shift keying (FSK) modulation) with the resulting spectrum having little dc energy. Since most of the distortion described in previous subsections is concentrated near dc, an analog ac-coupling filter, which is easily attainable by simple capacitive coupling, allows most of the noise near dc to be removed with minimal distortion to the signal spectrum. The simplicity of the capacitive coupling approach maintains the advantages of a DCR architecture. Therefore, DCR architectures with ac-coupling will be further explored in this paper. We assume that only a single ac-coupling filter is employed at the baseband. Cascading several ac-coupling filters with appropriate buffers in between them is also possible. Extension of the analysis method presented in this paper to multiple ac-coupling filters is straightforward.

For modulation schemes more spectrally efficient than the wide-band FSK, such as the pulse amplitude modulation (PAM), this simple method of ac-coupling the baseband signal before sampling introduces severe intersymbol interference (ISI) because of the large signal bearing spectrum near dc. The amount of ISI introduced increases with increasing ac-coupling cut-off frequency. With a wider notch, however, the time constant of the ac-coupling filter is smaller, resulting in faster response time. This effect is important for effectively attenuating the changing dc-offset values so to ensure subsequent baseband amplifiers from saturating. The selection of the ac-coupling cut-off frequency, therefore, requires a careful balance between two con-

flicting interests—minimizing ISI and maximizing immunity against the dc-offset noise.

Assuming that the dc-offset noise has been reduced to a negligible amount by the ac-coupling filter, the remaining ISI in a DCR with whitened matched filter is due to the ac-coupling filter and the $1/f$ noise (“colored noise” is equivalent in its effect to ISI). To minimize the effects of ISI, a water-filling PSD at the transmitter with an appropriate receive filter is optimal [13]. Optimality is defined in this context as maximizing the signal-to-noise ratio (SNR) as given in Section IV. A discrete version of this approach, which is vector coding (VC) [3], is asymptotically optimal for large vector dimensions. VC and its variations, however, are not effective at low vector dimensions and suffer from hardware complexity at large vector dimensions. Furthermore, exact knowledge of the channel response as well as the additive noise spectrum is required at the transmitter. Thus, VC is most effective for stationary or slowly varying channels, and it is generally not as effective in rapidly varying channels such as in wireless communication applications. Nonetheless, the performance of VC for large vector dimensions represents an upper bound of the performance attainable in a DCR and serves as a basis for comparison to other reception methods.

A finite-impulse response (FIR) minimum mean-square-error linear equalizer (MMSE-LE) can be employed to mitigate the effects of ISI in a DCR. A linear equalizer is simple and can be made to easily adapt to changing channel and noise conditions. Thus, FIR MMSE-LE is well suited for use in time-varying channels and robust to the $1/f$ roll-off frequency changes from temperature and process variations. At low SNR, FIR MMSE-LE performs well compared to VC, but performance degrades significantly with increasing SNR. To achieve high performance at large SNR, the transmitted signal spectrum can be modified to approximate the water-filling PSD solution for VC. Since distortion occurs primarily at low frequencies, the signal spectrum of VC has most of the signal-bearing energy concentrated at higher frequencies much like the spectrum for digital paging (wide-band FSK) without increasing the signal bandwidth. An approximation to this water-filling PSD can be obtained with negligible complexity by employing a simple line code with no energy at dc, such as the alternate-mark inversion (AMI) code. In Section IV-B, we demonstrate that using an MMSE-LE followed by maximum-likelihood sequence estimator (MLSE) designed only for AMI signal without any knowledge of the channel results in performance very close to asymptotic VC solution at realistic ac-coupling cut-off and $1/f$ roll-off frequencies. Furthermore, the number of filter taps required in MMSE-LE is minimal. Thus, the spectral shaping method retains the advantages of employing FIR MMSE-LE while achieving close to optimum VC performance at large SNR values.

In this paper, we limit our study to linear equalizers. Other equalizers, such as the decision-feedback equalizer and MLSE, are not considered.

III. SYSTEM MODEL

Our overall system model is shown in Fig. 4. The incoming bit stream b_l is encoded to generate x_k , where $x_k \in \{1, -1\}$.

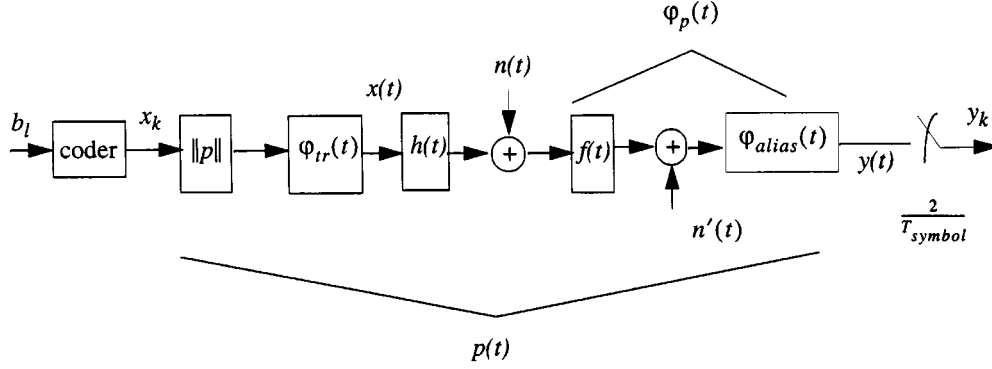


Fig. 4. Overall system model.

The discrete signal x_k is scaled by the magnitude of the transmit filter $\|p\|$ at a rate of $1/T_{\text{symbol}}$, then passed through a normalized transmit filter $\varphi_{tr}(t)$. The resulting transmit power is $\|p\|^2$. The transmit signal $x(t)$ is then filtered by the channel response $h(t)$. At the receiver end, the received signal is corrupted by additive noise $n(t)$, which consists of the $1/f$, dc-offset, and down-converted white Gaussian noise, before passing through an ac-coupling filter $f(t)$. The Fourier transform of $f(t)$ is given by

$$F(j\omega) = \frac{j\omega}{j\omega + 2\pi f_c} \quad (2)$$

where f_c is the cut-off frequency. The ac-coupled signal is further corrupted by white Gaussian noise $n'(t)$, which represents the input referred noise of the baseband amplifiers. The resulting corrupted signal is sampled at twice the symbol frequency, $T_{\text{sample}} = T_{\text{symbol}}/2$. An anti-alias filter precedes the sampling device, which is assumed to be an ideal lowpass filter with a gain transfer of $\sqrt{T_{\text{sample}}}$ over the frequency range of $-\pi/T_{\text{sample}} \leq \omega \leq \pi/T_{\text{sample}}$.

A. Signal and Noise Model

Referring to Fig. 4, the channel output signal just before the sampling device is

$$y(t) = \sum_m x_m \cdot p(t - mT_{\text{symbol}}) + n(t) \otimes \varphi_p(t) + n'(t) \otimes \varphi_{\text{alias}}(t) \quad (3)$$

where \otimes denotes convolution

$$\varphi_p(t) = \varphi_{\text{alias}}(t) \otimes f(t) \quad (4)$$

and the pulse response $p(t)$ is

$$p(t) = \|p\|(\varphi_{tr}(t) \otimes \varphi_p(t) \otimes h(t)). \quad (5)$$

We assume an ideal channel response of $h(t) = \delta(t)$. Sampling at time instant $t = kT_{\text{symbol}} - iT_{\text{symbol}}/2$, $i = 0, 1$, and k is an integer, (3) can be rewritten using vectors as

$$\mathbf{y}_k = \sum_m x_m \cdot \mathbf{p}_{k-m} + \mathbf{n}_k \quad (6)$$

where

$$\mathbf{y}_k = \begin{bmatrix} y(kT_{\text{symbol}}) \\ y\left(kT_{\text{symbol}} - \frac{T_{\text{symbol}}}{2}\right) \\ p(kT_{\text{symbol}}) \\ p\left(kT_{\text{symbol}} - \frac{T_{\text{symbol}}}{2}\right) \end{bmatrix} \quad (7)$$

and in (8), shown at the bottom of the page. The sampled pulse response \mathbf{p}_k is assumed to extend only a finite time interval $0 \leq t \leq vT_{\text{symbol}}$, where v is an integer, and any nonzero component of $p(t)$ outside this interval is assumed negligible. The interval is set in this paper such that the sampled response outside this interval is 50 dB smaller than the largest sample. Although such a description can never be exact in practice, this description can be very close to a realistic response of $p(t)$ if a sufficient number of samples are included. Thus, (6) becomes

$$\mathbf{y}_k = [\mathbf{p}_0 \quad \mathbf{p}_1 \quad \cdots \quad \mathbf{p}_v] \begin{bmatrix} x_k \\ x_{k-1} \\ \vdots \\ x_{k-v} \end{bmatrix} + \mathbf{n}_k. \quad (9)$$

$$\mathbf{n}_k = \begin{bmatrix} n(t) \otimes \varphi_p(t)|_{kT_{\text{symbol}}} + n'(t) \otimes \varphi_{\text{alias}}(t)|_{kT_{\text{symbol}}} \\ n(t) \otimes \varphi_p(t)|_{kT_{\text{symbol}} - T_{\text{symbol}}/2} + n'(t) \otimes \varphi_{\text{alias}}(t)|_{kT_{\text{symbol}} - T_{\text{symbol}}/2} \end{bmatrix} \quad (8)$$

More generally, for N_f successive two-tuple samples of $y(t)$,

$$\begin{aligned} \mathbf{Y}_{k, N_f} &\equiv \begin{bmatrix} \mathbf{y}_k \\ \mathbf{y}_{k-1} \\ \vdots \\ \mathbf{y}_{k-N_f+1} \end{bmatrix} \\ &= \begin{bmatrix} \mathbf{p}_0 & \mathbf{p}_1 & \cdots & \mathbf{p}_v & 0 & \cdots & 0 \\ 0 & \mathbf{p}_0 & \mathbf{p}_1 & \cdots & \mathbf{p}_v & \cdots & 0 \\ \vdots & \vdots & \vdots & \vdots & \vdots & \vdots & \vdots \\ 0 & \cdots & 0 & \mathbf{p}_0 & \mathbf{p}_1 & \cdots & \mathbf{p}_v \end{bmatrix} \\ &\quad \cdot \begin{bmatrix} x_k \\ x_{k-1} \\ \vdots \\ x_{k-N_f-v+1} \end{bmatrix} + \begin{bmatrix} \mathbf{n}_k \\ \mathbf{n}_{k-1} \\ \vdots \\ \mathbf{n}_{k-N_f+1} \end{bmatrix} \\ &= \mathbf{P}_{N_f} \cdot \mathbf{X}_{k, N_f} + \mathbf{N}_{k, N_f} \end{aligned} \quad (10)$$

where \mathbf{P}_{N_f} denotes the pulse matrix, \mathbf{X}_{k, N_f} the data vector, and \mathbf{N}_{k, N_f} the noise vector.

B. Noise Autocorrelation Function

Additive noise $n(t)$ consists of three independent noise sources: dc-offset noise $n_{dc}(t)$, white Gaussian noise $n_{wg}(t)$, and $1/f$ noise $n_{1/f}(t)$

$$n(t) = n_{dc}(t) + n_{wg}(t) + n_{1/f}(t). \quad (11)$$

The white Gaussian noise $n_{wg}(t)$ is the output referred noise of the RF and down-conversion stages. Assuming power gains of 25 dB and noise figure of 5 dB in the RF and down-conversion stages, the PSD of $n_{wg}(t)$, denoted as $P_{n_{wg}}(j\omega)$, is 30 dB above the thermal noise floor. The PSD of $n'(t)$ ($P_{n'}(j\omega)$), which represents the input referred noise of the baseband amplifiers, is assumed to be 20 dB above the thermal noise floor. Thus, the PSD of $n'(t)$ is 10 dB below that of $n(t)$.

Assuming stationarity (which is explained further shortly) and given the independence of the four noise sources $n_{wg}(t)$, $n_{dc}(t)$, $n_{1/f}(t)$, and $n'(t)$, the sampled noise autocorrelation function $R_n(\beta)$ is given by

$$R_n(\beta) = R_{n_{wg}}(\beta) + R_{n_{dc}}(\beta) + R_{n_{1/f}}(\beta) + R_{n'}(\beta) \quad (12)$$

where β is an integer and the subscript denotes a particular noise source.

The ac-coupling filter cut-off frequency should be made wide enough to effectively remove the variation of the dc-offset noise to prevent saturation of the baseband amplifiers. Thus, we assume that the ac-coupling filter attenuates the dc-offset noise $n_{dc}(t)$ such that its resulting PSD is substantially lower than that of $n'(t)$, allowing an approximation of $R_{n_{dc}}(\beta) \approx 0$ for all β regardless of the magnitude of the dc-offset.

Filtering nonstationary flicker noise $n_{1/f}(t)$ by $f(t)$ allows $n_{1/f}(t)$ to be modeled as colored stationary noise. Since the power spectrum of the ac-coupling filter falls at -20 dB/decade and the $1/f$ noise rises at 10 dB/decade with decreasing frequency, the energy of $1/f$ noise filtered by $\varphi_p(t)$ becomes negligible for frequencies much smaller than both the $1/f$ roll-off frequency and the ac-coupling cut-off frequency. Consequently, approximating the $1/f$ noise spectrum using $H(j\omega)$ given in (1) for three or more decades below the $1/f$ noise does not alter $R_{n_{1/f}}(\beta)$ values for all β . Thus, we model the $1/f$ noise with $m = 5$ and $e = 3$ dB in (1), which corresponds to approximating the $1/f$ noise spectrum for six decades below the $1/f$ roll-off frequency.

With the approximation $R_{n_{dc}}(\beta) \approx 0$ and modeling the $1/f$ noise using (1), (12) can be written as

$$R_n(\beta) = \frac{T_{\text{sample}}}{2\pi} \int_{-\pi/T_{\text{sample}}}^{\pi/T_{\text{sample}}} (P_{n_{wg}}(j\omega) + |H(j\omega)|^2) |F(j\omega)|^2 \cdot e^{j\omega\beta T_{\text{sample}}} d\omega + P_{n'}(0)\delta(\beta) \quad (13)$$

where $\delta(\cdot)$ is a unit sample sequence.

IV. PERFORMANCE ANALYSIS

The performance of a DCR is measured by determining the loss in SNR compared to that of an ideal receiver. SNR is defined as

$$\text{SNR} \equiv \frac{1}{E\{|x_k - \hat{x}_k|^2\}} \quad (14)$$

where \hat{x}_k is the receiver estimate of the transmitted symbol x_k . An ideal receiver is a receiver that does not suffer from the $1/f$ noise and dc-offset noise and, consequently, does not require an ac-coupling filter $f(t)$. The SNR of an ideal receiver is

$$\text{SNR}_{\text{ideal}} = \frac{\|p\|^2}{P_{n_{wg}}(0) + P_{n'}(0)}. \quad (15)$$

For simplicity and without loss of generality, we assume that the transmit filter $\varphi_{tr}(t)$ is a Nyquist square-root raised-cosine filter with a roll-off factor of 0.5.

A. Optimum DCR Performance

VC operates by processing $N+v$ blocks of channel input at a time, where $v+1$ is the length of the sampled channel pulse response. The modulator in VC then creates a set of basis vectors that remain orthogonal after undergoing the dispersive effects of the ISI channel, resulting in a set of N independent parallel channels. This is obtained by performing a singular value decomposition of the whitened pulse response matrix, that is

$$R_{N_{N_f} N_{N_f}}^{-1/2} \mathbf{P}_N = F[\Lambda \ 0] M^* \quad (16)$$

where $*$ denotes complex conjugation, \mathbf{P}_N is the pulse response matrix given in (10), Λ is a diagonal matrix of singular values,

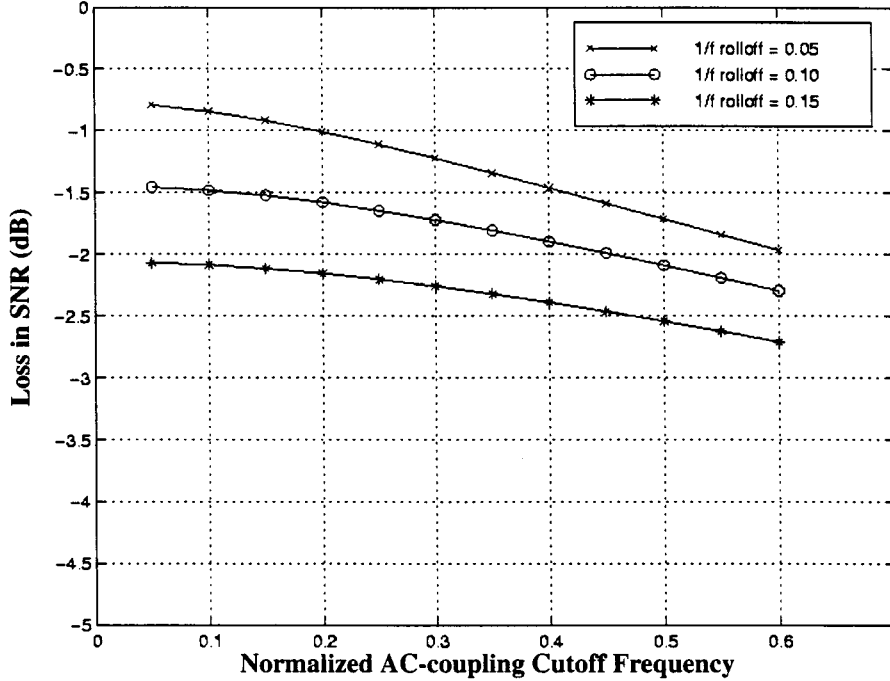


Fig. 5. SNR loss to ideal receiver versus ac-coupling cut-off frequency for VC ($N = 600$).

and F and M are unitary matrices. $R_{\mathbf{N}_{N_f} \mathbf{N}_{N_f}}^{1/2}$ is a (nonunique) square root of $R_{\mathbf{N}_{N_f} \mathbf{N}_{N_f}}$, which is given by

$$R_{\mathbf{N}_{N_f} \mathbf{N}_{N_f}} = \begin{bmatrix} R_n(0) & R_n(1) & \cdots & R_n(2N_f) \\ R_n(1) & R_n(0) & \cdots & R_n(2N_f - 1) \\ \vdots & \vdots & \ddots & \vdots \\ R_n(2N_f) & \cdots & \cdots & R_n(0) \end{bmatrix} \quad (17)$$

where $R_n(\cdot)$ is computed numerically using (13). Selecting the transmit filter as M and receive filter as F^* results in N parallel independent channels

$$\mathbf{Y}_{k,N} = \Lambda \cdot \mathbf{X}_{k,N} + \mathbf{N}_{k,N}. \quad (18)$$

A water-fill energy allocation using loading algorithms such as proposed by Aslanis [11] to this set of parallel channels with an energy constraint $\|p\|^2$ and a capacity “gap” Γ maximizes the SNR of the multiple parallel channels, which is given as

$$\text{SNR} = \left[\left(\prod_{n=1}^N \left[1 + \frac{\text{SNR}_n}{\Gamma} \right] \right)^{1/(N+v)} - 1 \right] \cdot \Gamma \quad (19)$$

where SNR_n is the SNR of each channel. For $\Gamma = 8.23$ dB, which corresponds to $\text{SNR}_{\text{ideal}} = 13$ dB with no error-correction code, the loss in SNR compared to an ideal superheterodyne receiver, that is, $\text{SNR} - \text{SNR}_{\text{ideal}}$ is plotted in Fig. 5 for normalized $1/f$ roll-off frequencies of 0.05, 0.10, and 0.15 against normalized ac-coupling cut-off frequencies. The $1/f$ roll-off and ac-coupling cut-off frequencies are normalized to the symbol rate $1/T_{\text{symbol}}$. A vector dimension of $N = 600$ is selected.

With increasing ac-coupling cut-off frequency, the loss in SNR increases because of increasing ISI. The difference in SNR among the three $1/f$ roll-off frequencies is slightly

greater at lower ac-coupling cut-off frequencies than at higher frequencies. This is because the ISI contribution by the $1/f$ noise becomes relatively less significant compared to the contribution by the ac-coupling filter with increasing cut-off frequencies. In fact, as the ac-coupling cut-off frequency is increased further than shown in Fig. 5, the three plots eventually converge; this convergence implies that the ISI contribution by the ac-coupling filter dominates that of the $1/f$ noise. For normalized ac-coupling cut-off frequencies under 0.60, the difference in SNR among the three $1/f$ roll-off frequencies are approximately constant. For every increase in the normalized $1/f$ roll-off frequency of 0.05, performance degrades by roughly 0.5 dB.

A vector dimension of at least several hundred is necessary to achieve near VC asymptotic performance. Thus, the plots in Fig. 5 with $N = 600$ represent near-optimal performance attainable by a DCR. Although the performance of VC is optimal for large N , an important disadvantage associated with large vector dimension is the increase in complexity when measured in terms of operations per second and the size of the storage memory required. The number of computations can be reduced by as much as $N/\log N$ by approximating VC as N increases with discrete-multitone. However, the large memory requirement, which is often one of the largest source of power consumption in DSP chips [5], is difficult to reduce. Another drawback of large N is the longer latency in processing necessary, which is unacceptable in certain real-time applications. The time-domain equalizer, which is not addressed in this paper, partially alleviates some of these problems associated with large N by reducing the effective length of v [13].

Although the performance of VC in Fig. 5 represents near-optimum performance of a DCR given the $1/f$ roll-off and ac-coupling cut-off frequencies, a major disadvantage of VC is that the

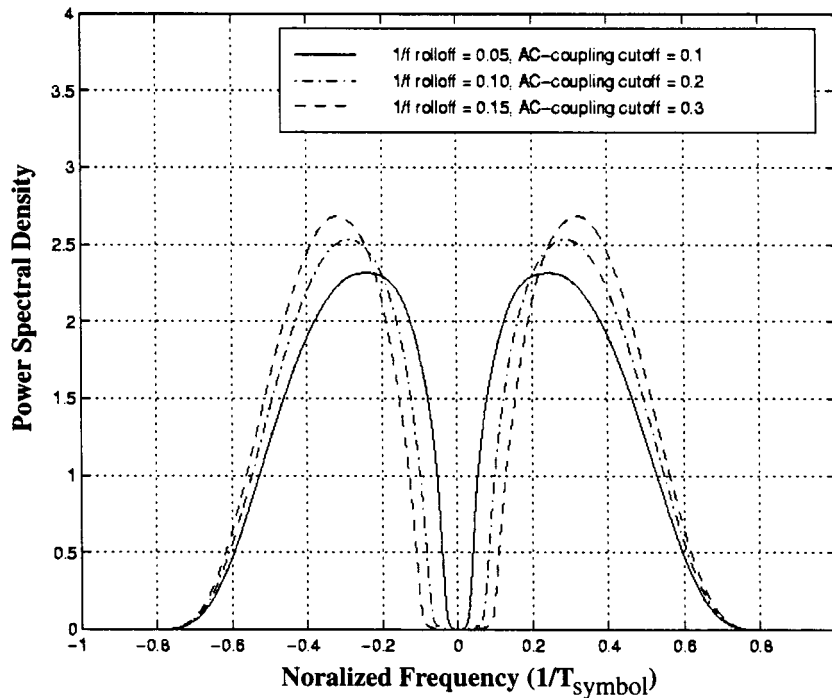


Fig. 6. Power spectrum of VC for square-root raised-cosine roll-off factor of 0.5.

channel and the noise spectrum need to be known at the transmitter. This is not always possible, especially in rapidly varying channels such as in the wireless environment. Nonetheless, VC serves as an upper bound and the basis of comparison with other adaptive reception methods discussed in subsequent sections. VC or its variations is probably most effectively employed with DCR in a near-stationary wired communication channel.

B. FIR MMSE-LE

The major advantages of FIR linear equalizer are that it is simple and easily adaptable to changing channel and noise conditions. Simple filtering of the received signal performs matched filtering, noise whitening, and channel equalization. No storage or buffering of the received signal is necessary. Since adaptive equalizers are often implemented with FIR structures, the channel response and the exact statistics of the noise need not be known *a priori*. This allows adaptation to rapidly varying channels as in a wireless environment. The adaptive convergence properties of FIR MMSE-LE in a DCR are not studied in this paper. We assume knowledge of the channel response and the noise statistics at the receiver.

Since the received signal \mathbf{y}_k is oversampled, an FIR MMSE-LE incorporates matched filtering, noise whitening, and channel equalization operations. The unbiased SNR for FIR MMSE-LE is [12]

$$\text{SNR}_{\text{MMSE-LE}, u} = \frac{1}{1 - \mathbf{w} \mathbf{R}_{x\mathbf{Y}_{N_f}}^*} \quad (20)$$

where \mathbf{w} is the equalizer of length N_f symbol periods with system delay of $\Delta \cdot T_{\text{symbol}}$ and

$$\mathbf{R}_{x\mathbf{Y}_{N_f}} = E \left\{ x_{k-\Delta} \mathbf{Y}_{k, N_f}^* \right\}. \quad (21)$$

Using orthogonality principles, \mathbf{w} is given by

$$\mathbf{w} = \mathbf{R}_{x\mathbf{Y}_{N_f}} \mathbf{R}_{\mathbf{Y}_{N_f} \mathbf{Y}_{N_f}}^{-1} \quad (22)$$

and

$$\begin{aligned} \mathbf{R}_{\mathbf{Y}_{N_f} \mathbf{Y}_{N_f}} &= E \left\{ \mathbf{Y}_{k, N_f} \mathbf{Y}_{k, N_f}^* \right\} \\ &= \mathbf{P}_{N_f} \cdot E \left\{ \mathbf{X}_{k, N_f} \mathbf{X}_{k, N_f}^* \right\} \cdot \mathbf{P}_{N_f}^* \\ &\quad + E \left\{ \mathbf{N}_{k, N_f} \mathbf{N}_{k, N_f}^* \right\} \\ &= \mathbf{P}_{N_f} \cdot \mathbf{R}_{\mathbf{X}_{N_f} \mathbf{X}_{N_f}} \cdot \mathbf{P}_{N_f}^* + \mathbf{R}_{\mathbf{N}_{N_f} \mathbf{N}_{N_f}} \end{aligned} \quad (23)$$

where $\mathbf{R}_{\mathbf{N}_{N_f} \mathbf{N}_{N_f}}$ is given in (17) and $\mathbf{R}_{\mathbf{X}_{N_f} \mathbf{X}_{N_f}}$ is an autocorrelation matrix of x_k .

1) *Fixed Transmitter*: If the designer has no control over the transmitted signal, the transmitted signal x_k is modeled as white. $\mathbf{R}_{\mathbf{X}_{N_f} \mathbf{X}_{N_f}}$ in (23) is then an identity matrix. The unbiased SNR in (20) is now readily computed given $\text{SNR}_{\text{ideal}}$.

2) *Spectral Shaping Using Line Codes*: Since signal distortion in a DCR occurs primarily at low frequencies, the water-filling PSD solution for VC is generally similar for all realistic ac-coupling cut-off and $1/f$ roll-off frequencies. Several examples of the power spectrum of VC are shown in Fig. 6. Most of the signal-bearing energy is allocated to energies above the $1/f$ roll-off and ac-coupling cut-off frequencies with negligible energy below them. Without requiring large vector dimensions, which introduces complexity and latency, the spectrum that approximates the optimal water-fill solution is obtained by employing a line code which minimizes energy at dc. An example of such line codes is the AMI code, which uses three levels to represent a bit. Although a binary line code is selected to demonstrate the advantages of this approach, line codes for large alphabets [6] with minimal energy at low frequencies can also be used. The spectral shaping in an AMI code is accomplished

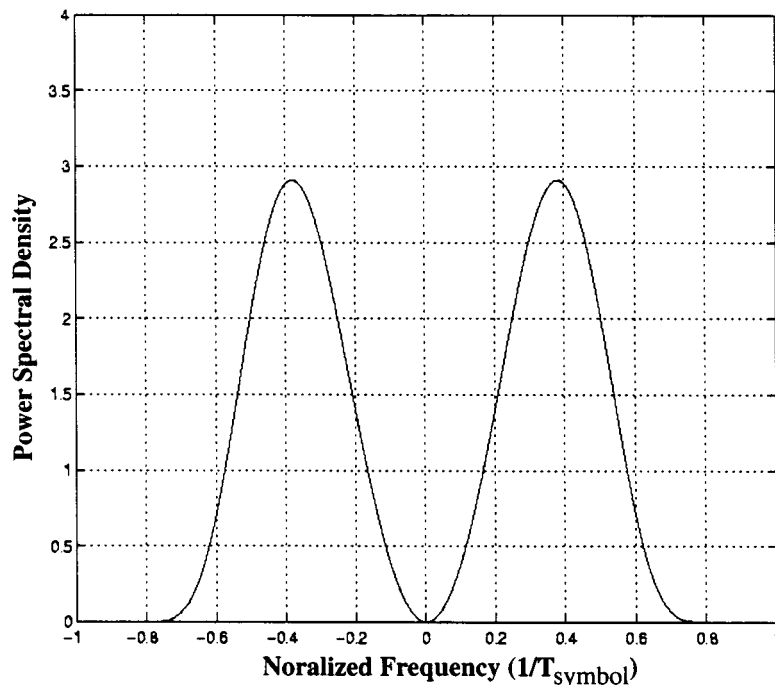


Fig. 7. Power spectrum of AMI code for square-root raised-cosine roll-off factor of 0.5.

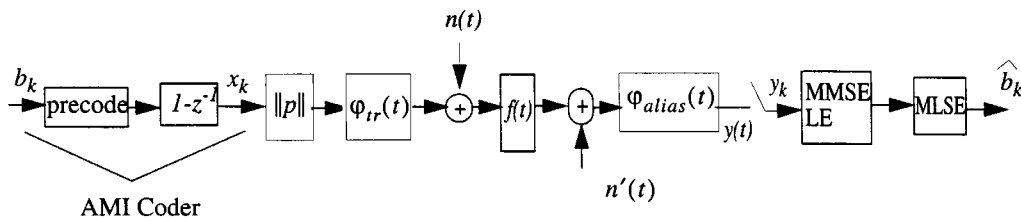


Fig. 8. System model for AMI with MLSE.

by introducing a $1 - z^{-1}$ filter at the transmitter. Precoding eliminates error propagation at the receiver. The signal power spectrum of the AMI code is illustrated in Fig. 7. Because the AMI code contains little signal-bearing energy at low frequencies, FIR MMSE-LE for the AMI code efficiently equalizes the received signal since it does not need to equalize the noisy low frequency energy components. Although the transmitted signal bandwidth remains constant, the use of AMI code requires additional transmit power because of the expanded alphabet. If an MLSE for AMI code is employed at the receiver, this performance loss due to alphabet expansion of the AMI code reduces to small amounts.

A block diagram of the AMI coder and the corresponding receiver is illustrated in Fig. 8. The received signal $y(t)$, which is oversampled at $2/T_{\text{symbol}}$, is equalized using an MMSE-LE. For an MMSE-LE of length N_f symbol periods, $R_{\mathbf{x}_{N_f} \mathbf{x}_{N_f}}$ is the autocorrelation matrix of AMI code [7] and is given by

$$R_{\mathbf{x}_{N_f} \mathbf{x}_{N_f}} = \begin{bmatrix} 1 & -0.5 & 0 & \cdots & 0 \\ -0.5 & 1 & -0.5 & \cdots & 0 \\ 0 & -0.5 & 1 & \cdots & 0 \\ \vdots & \vdots & \vdots & \ddots & \vdots \\ 0 & 0 & 0 & -0.5 & 1 \end{bmatrix}. \quad (24)$$

Equation (24) assumes that the bit stream b_k is equiprobable and independent from sample to sample. The equalized signal is then decoded using an MLSE designed only on knowledge of the AMI code. The MLSE requires two states.

The unbiased SNR of an equalized AMI code with MLSE is obtained by resorting to a Monte Carlo simulation for each possible combination of $1/f$ roll-off and ac-coupling cut-off frequencies and $\text{SNR}_{\text{ideal}}$ values. Computing the error probability of MLSE using the minimum Euclidean distance between the transmitted and the incorrect sequence as in [8] is not accurate since the noise at the output of MMSE-LE is colored. With colored noise, error events with the same squared Euclidean distance affect error probability differently since the order of the error sequence also impacts the error probability [9]. Thus, the performance results are obtained by computer simulation. The probability of error obtained by simulation is then converted using the inverse error function to a corresponding SNR in an AWGN channel for comparison to the previously presented decoding methods.

3) *Performance Results of FIR MMSE-LE:* The SNR loss is plotted in Fig. 9 against normalized cut-off frequency when direct-conversion is performed for both approaches described above—MMSE-LE assuming transmitted signal is white and MMSE-LE/MLSE assuming transmitted signal is AMI coded. Fig. 9 plots performance loss for normalized $1/f$ roll-off

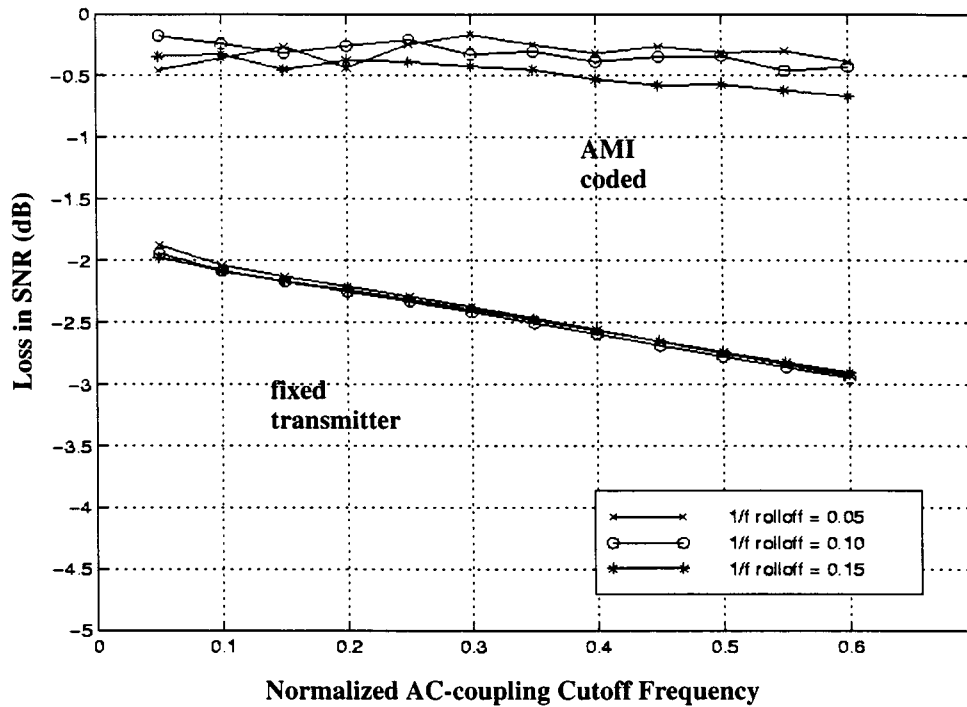


Fig. 9. SNR loss to optimal direct-conversion versus ac-coupling cut-off frequency for FIR-MMSE-LE ($N = 25$).

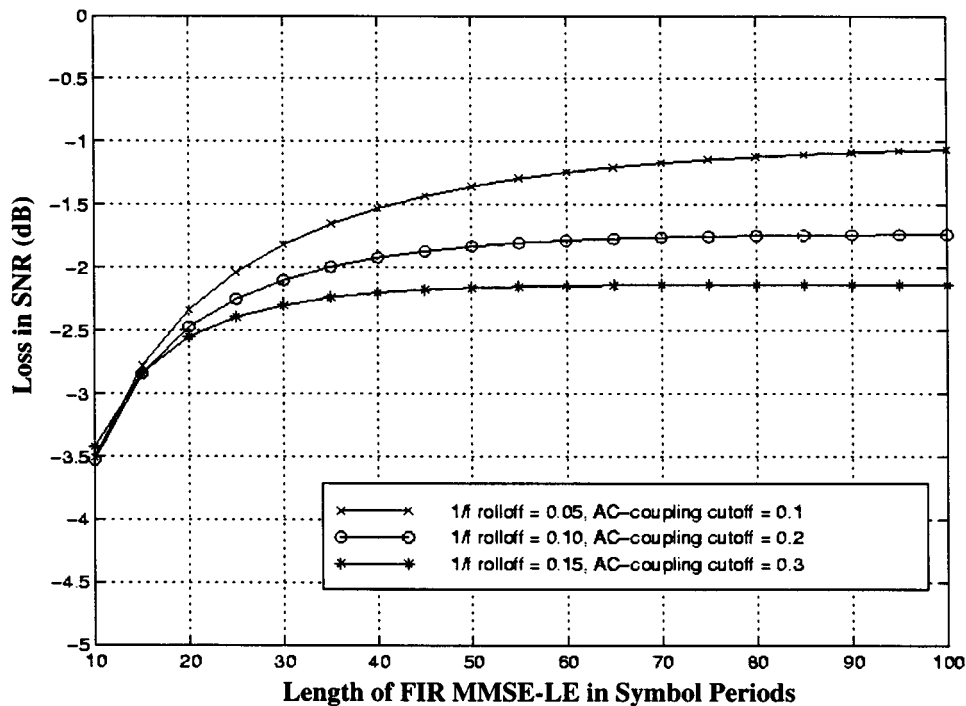


Fig. 10. SNR loss to optimal direct-conversion versus length of MMSE-LE for fixed transmitter.

frequencies of 0.05, 0.10, and 0.15. Both approaches perform matched filtering, noise whitening, and channel equalization using FIR MMSE-LE with $N_f = 25$. The SNR loss is with respect to optimal DCR obtained using VC as in Fig. 5 when $\text{SNR}_{\text{ideal}} = 13$ dB. The unbiased SNR of an equalized AMI code with MLSE is obtained by simulating each combination with 10^8 samples. For both approaches, the SNR loss compared to asymptotic VC performance is insensitive to the $1/f$ roll-off

frequencies. Without AMI code, the SNR loss steadily worsens with increasing ac-coupling cut-off frequency from 2 to 3 dB for normalized cut-off frequencies of 0.1 to 0.6, respectively; whereas, the SNR loss with AMI code remains approximately constant at under 0.5 dB.

The complexity and power consumption of a linear equalizer are strongly dependent on the number of FIR filter taps. The effect of symbol periods on FIR MMSE-LE assuming that the

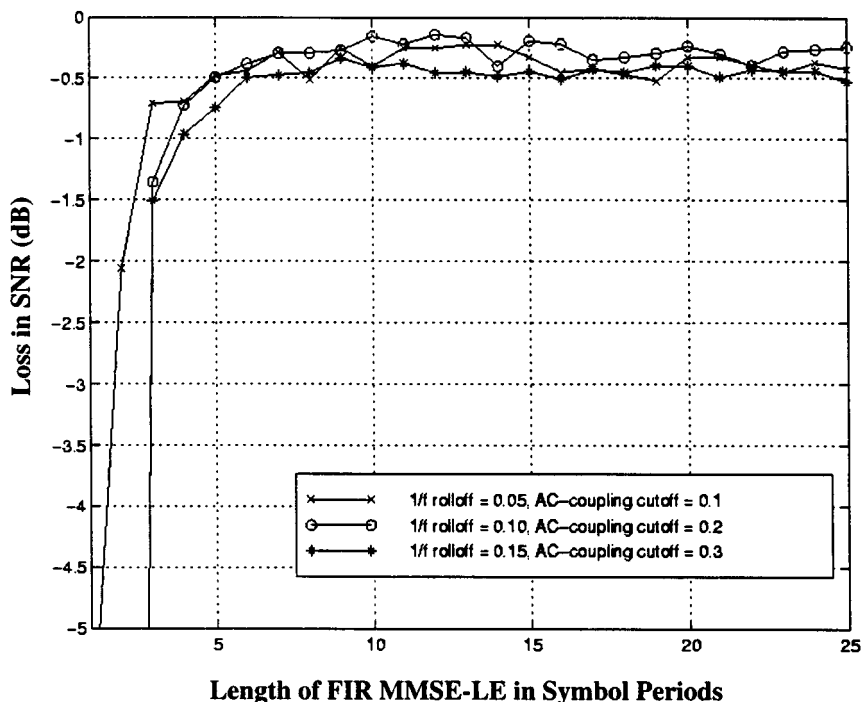


Fig. 11. SNR loss to optimal direct-conversion versus length of MMSE-LE for AMI/MMSE-LE/MLSE.

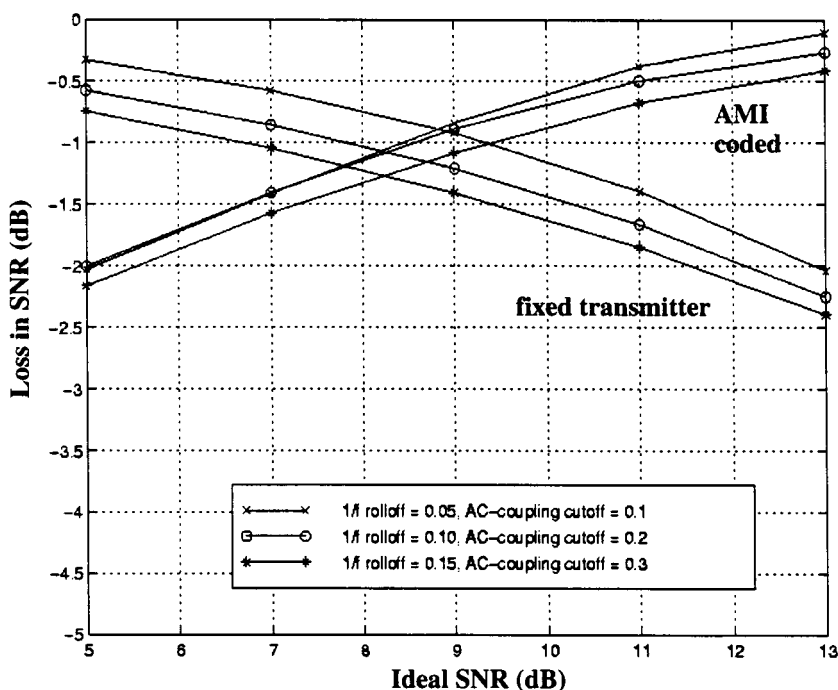


Fig. 12. SNR loss to optimal direct-conversion versus ideal SNR ($N = 25$).

transmitted signal is white and $SNR_{ideal} = 13$ dB is shown in Fig. 10. The SNR loss is with respect to VC of $N = 600$. The plots corresponding to smaller $1/f$ roll-off and ac-coupling cut-off frequencies saturate more slowly. This is because the channel impulse response is longer, requiring more filter taps to equalize. When the normalized $1/f$ roll-off and ac-coupling cut-off frequencies are 0.05 and 0.1, respectively, over 40 symbol periods are required to perform within 0.5 dB of the infinite-length equalizer performance.

The effect of the filter length on AMI/MMSE-LE/MLSE when $SNR_{ideal} = 13$ dB is shown in Fig. 11. The number of filter taps required to achieve near infinite-length equalizer performance is under $N_f = 8$, which is substantially less than an equalizer without the AMI code. The reason for the shorter filter taps is that the MMSE-LE for an AMI code does not attempt to flatten the spectrum of the received signal, since only little signal-bearing energy exists at low frequencies. Thus, the equalizer for an AMI need not remember the low frequency

distortion introduced by the ac-coupling filter and the $1/f$ noise, resulting in fewer filter taps. The small number of filter taps required allows this reception method to be simple and hardware efficient.

The effect of the variation in $\text{SNR}_{\text{ideal}}$ when the filter length is 25 symbol periods is illustrated in Fig. 12. Both approaches are plotted for normalized $1/f$ roll-off frequencies of 0.05, 0.10, and 0.15. The SNR loss is with respect to VC of $N = 600$. At $\text{SNR}_{\text{ideal}}$ less than 9 dB, MMSE-LE without AMI code is effective. The AMI/MMSE-LE/MLSE approach is not effective at low $\text{SNR}_{\text{ideal}}$, since the increased number of nearest neighbors in MLSE dominates the error probability [7]. For applications with $\text{SNR}_{\text{ideal}}$ values greater than 9 dB or with low probability of error requirements, however, AMI/MMSE-LE/MLSE is effective.

C. Design Example

An example of a DCR design is provided. The following assumptions are made.

- 1) Symbol rate of BPSK is 100 kHz with raised-cosine roll-off parameter of 0.5.
- 2) The $1/f$ roll-off frequency is 5 kHz.
- 3) The PSD of $n_{\text{wg}}(t)$ is 10 dB greater than the PSD of $n'(t)$.
- 4) The bandwidth of the worst-case dc-offset noise is 20 Hz and its PSD is at most 40 dB greater than the PSD of $n_{\text{wg}}(t)$.

The cut-off frequency of the ac-coupling filter is determined by the magnitude of the dc-offset noise and the rate at which the dc-offset noise changes, which is approximately its bandwidth. We assume a brickwall PSD for the dc-offset noise with a bandwidth of 20 Hz. The ac-coupling filter should attenuate the dc-offset noise so that it is negligible relative to $n'(t)$. We require that the PSD of dc-offset noise be suppressed to at least 4 dB below the PSD of $n'(t)$. This implies a 54-dB attenuation of the dc-offset noise at 20 Hz, requiring an ac-coupling filter with a corner frequency of 10 kHz or a normalized corner frequency of 0.1.

From Fig. 5, the performance loss of an optimal DCR with a normalized ac-coupling cut-off frequency of 0.1 and a normalized $1/f$ roll-off frequency of 0.05 is approximately 0.8 dB compared to an ideal superheterodyne receiver when $\text{SNR}_{\text{ideal}} = 13$ dB. Using Fig. 9, the performance loss of FIR MMSE-LE with $N = 25$ and without spectral shaping is approximately 2.1 dB compared to an optimal DCR. With the same equalizer but with the AMI code and MLSE, the performance loss is only 0.3 dB. Compared to an ideal superheterodyne receiver, a DCR with and without AMI code suffers an SNR loss of 1.1 and 2.9 dB, respectively.

In this example, the cut-off frequency of the ac-coupling filter is 10 kHz, which may require a capacitor that is too large for on-chip integration. To reduce the required capacitance, the DCR may choose a higher cut-off frequency than necessary at the expense of reduced performance. For example, if the corner frequency is selected to be 40 kHz, there is a total SNR loss compared to an ideal superheterodyne receiver of approximately 1.8 and 4.1 dB for a DCR with and without AMI code, respectively, as inferred from Figs. 5 and 9.

V. CONCLUSIONS

DCRs are well suited for reception in a portable wireless environment, where power, cost, and size are critical design constraints. Although VC achieves the best performance for large vector dimensions, it is inappropriate for a rapidly changing wireless channel environment because the effective use of VC requires knowledge of the channel response at the transmitter. Furthermore, VC suffers from large hardware complexity as explained in Section IV-A. However, FIR linear equalizers in section Section IV-B are simpler and can be readily modified to adaptively equalize both the channel $h(t)$ and the distortion contributed by the use of a direct-conversion architecture. Thus, an FIR equalizer is a more desirable decoding approach in a rapidly varying channel. Although linear equalizer performs well at low $\text{SNR}_{\text{ideal}}$, its performance degrades significantly at larger $\text{SNR}_{\text{ideal}}$. To achieve the high performance of VC while maintaining the adaptability and low complexity of an FIR equalizer even at high $\text{SNR}_{\text{ideal}}$, the use of line codes is proposed. The performance of this suboptimal approach is very close to an infinite-dimensional VC with minimal complexity.

The work presented in this paper should serve as a basis for future research in improving the performance of DCRs. The effectiveness of other line codes or combination of line and error-correction codes with various equalization and detection methods for DCRs deserves further investigation.

It is unlikely that a DCR will perform as well as a well-designed superheterodyne-based receiver that is free of the $1/f$ and dc-offset noise. The significant reduction in cost, size, and power consumption achieved when a direct-conversion architecture is employed, however, might prove to be more critical in many communication applications.

APPENDIX

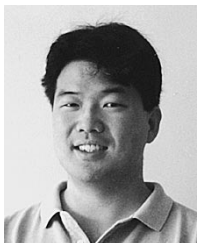
Given x_0 and e , the allowed approximation error in decibels, in Fig. 3, p_i , z_i , and x_i can be computed recursively. The following equations are obtained by applying elementary geometry:

$$\begin{aligned} 10 \cdot \log(p_i) &= 10 \cdot \log(x_i) - e \\ 10 \cdot \log(z_i) &= 10 \cdot \log(x_i) + e \\ 10 \cdot \log(x_{i+1}) &= -30 \cdot \log(x_i) + 40 \cdot \log(p_i). \end{aligned}$$

REFERENCES

- [1] A. Abidi, "Direct-conversion radio transceivers for digital communications," *IEEE J. Solid-State Circuits*, vol. 30, pp. 1399–1410, Dec. 1995.
- [2] J. Wilson *et al.*, "A single-chip VHF and UHF receiver for radio paging," *IEEE J. Solid-State Circuits*, vol. 26, pp. 1944–1950, Dec. 1991.
- [3] J. A. C. Bingham, "Multicarrier modulation for data transmission: An idea whose time has come," *IEEE Commun. Mag.*, pp. 5–14, Apr. 1990.
- [4] P. Estabrook *et al.*, "The design of a mobile radio receiver using a direct conversion architecture," in *Proc. IEEE Vehicular Technology Conf.*, San Francisco, May 1989, pp. 63–72.
- [5] T. Meng *et al.*, "Portable video-on-demand in wireless communications," *Proc. IEEE*, vol. 83, pp. 659–680, Apr. 1995.
- [6] A. R. Calderband and J. E. Mazo, "Spectral nulls and coding with large alphabets," *IEEE Commun. Mag.*, pp. 58–67, Dec. 1991.
- [7] E. Lee and D. Messerschmitt, *Digital Communication*, 2nd ed., Norwell, MA: Kluwer, 1994.
- [8] J. Proakis, *Digital Communications*, 2nd ed., New York: McGraw-Hill, 1989.

- [9] J. Wang and H. Chung, "Trellis coded communication systems—Colored noise and the swapping technique," *IEEE Trans. Commun.*, vol. 38, pp. 1549–1556, Sept. 1990.
- [10] D. Haspeslagh *et al.*, "BBTRX: A baseband transceiver for a zero IF GSM hand portable station," in *Proc. Custom IC Conf.*, San Diego, CA, 1992, pp. 10.7.1–10.7.4.
- [11] J. T. Aslanis Jr. *et al.*, "Achievable information rates on digital subscriber loops: Limiting information rates with crosstalk noise," *IEEE Trans. Commun.*, vol. 40, pp. 361–372, Feb. 1992.
- [12] J. Cioffi, "Data signals, sets, and detection," Stanford Univ., Stanford, CA, EE379a class notes.
- [13] —, "Channel dependent data signals," Stanford Univ., Stanford, CA, EE379c class notes.
- [14] B. Razavi, "RF IC design challenges," in *Proc. Design Automation Conf.*, San Francisco, CA, 1998, pp. 408–413.



Won Namgoong (S'95–M'99) received the B.S. degree in electrical engineering and computer sciences from the University of California at Berkeley in 1993, and the M.S. and Ph.D. degrees from Stanford University, Stanford, CA, in 1995 and 1999, respectively.

In 1999, he joined the faculty of the Electrical Engineering–Systems Department at the University of Southern California, Los Angeles, where he is an Assistant Professor. His current research activities include communication transceivers, signal processing systems, and low-power/high-speed circuits.

Dr. Namgoong received the Stanford University School of Engineering Fellowship in 1993 and the Korea Foundation for Advanced Studies Fellowship in 1997.



Teresa H. Meng (S'82–M'88–SM'93–F'99) received the B.S. degree from National Taiwan University, Taiwan, R.O.C., in 1983, and the M.S. and Ph.D. degrees from the University of California at Berkeley in 1984 and 1988, respectively.

She joined the faculty of the Electrical Engineering Department at Stanford University, Stanford, CA, in 1988, where she is an Associate Professor. Her current research activities include low-power circuit design, wireless networks, and portable DSP systems.

Dr. Meng was Co-Program Chair of the 1992 Application Specific Array Processor Conference and of the 1993 HOTCHIP Symposium. She also served as General Chair of the 1996 IEEE Workshop on VLSI Signal Processing. She is the recipient of the IEEE Signal Processing Society's Paper Award in 1989, the 1989 National Science Foundation Presidential Young Investigator Award, the 1989 ONR Young Investigator Award, a 1989 IBM Faculty Development Award, and the 1988 Eli Jury Award from U.C. Berkeley for recognition of excellence in systems research.